Crew Exploration Vehicle Composite Pressure Vessel Thermal Assessment

Laurie Y. Carrillo[1], Ángel R. Álvarez-Hernández[2], and Steven L Rickman[3]
NASA Johnson Space Center (JSC), Houston, TX 77058

The Crew Exploration Vehicle (CEV) is the next generation space vehicle to follow the Space Shuttle. A design with the inclusion of a Composite Pressure Vessel (CPV) has been assessed for its thermal response. The temperature distribution on the CPV that results from the heat produced by internal spacecraft systems and external space environments was calculated as part of a project-level assessment to understand thermomechanical stresses. A finite element translation of the crew module CPV was integrated into an existing CEV Thermal Math Model (TMM) based on the 605 baseline configuration and analyzed for four orbital cases. Steady state temperature profiles were generated based on orbit average heating. Preliminary thermal analysis results suggest that the CPV requires less make-up energy when compared to the baseline aluminum pressure vessel. It is emphasized that only local make-up energy was considered in the study. The make-up energy did not include the zoning configuration that occurs with heaters. This document presents the approach and assumptions used for this thermal assessment.

I. Introduction

In an effort to increase NASA's expertise in the area of composite structures, the NASA Engineering and Safety Center (NESC) undertook a project to design, analyze and fabricate a pathfinder composite crew module. The NESC's proposed composite material design differs from the current Crew Exploration Vehicle (CEV) baseline in which an aluminum pressure vessel is used. As part of the effort, the design and anticipated performance were studied through analysis. One of the vital areas to understand in spacecraft analysis is the resulting thermal performance of the vehicle when exposed to the unique environment of space coupled with the heat produced from the spacecraft's myriad of internal systems. The resulting thermal performance is dependent on a complex combination of factors that include the thermophysical and optical properties of the many materials that compose the spacecraft, the orientation of the spacecraft in orbit with respect to nearby radiating bodies such as the earth, sun and moon, and the power dissipation of the internal systems. This paper describes the thermal analysis performed with the aim of providing a means by which to begin a thermomechanical stress investigation of the spacecraft.

A finite element representation of the CPV was imported into the JSC-built CEV Thermal Math Model (TMM) based on the 605 baseline configuration utilizing the Systems Improved Numerical Differencing Analyzer (SINDA) program for heat transfer calculations. This model includes CEV's Backshell (BS), Heatshield (HS), structural heat transfer paths of the Thermal Protection System (TPS), Service Module (SM) and Low Impact Docking System (LIDS). The on-orbit thermal environments were calculated and the internal subsystem heat dissipation was included. Internal convection couplings were modeled. The required energy applied to specific locations within the CPV to maintain the temperature above the dewpoint has been defined as the local make-up energy. A broad assessment of local make-up energy requirements is conducted as a preliminary step toward determining the required input power. The rigorous zoning configuration specifications required to fully determine internal heater power is relegated to a further study. Steady state temperature profiles have been produced based on orbit average heating.

[1] Aerospace Engineer, NASA Johnson Space Center, Structural Engineering Division, Thermal Design Branch, 2101 NASA Pkwy, Houston, TX 77058
[2] Aerospace Engineer, NASA Johnson Space Center, Structural Engineering Division, Thermal Design Branch, 2101 NASA Pkwy, Houston, TX 77058
[3] Thermal Design Branch Chief, NASA Johnson Space Center, Structural Engineering Division, Thermal Design Branch, 2101 NASA Pkwy, Houston, TX 77058

This paper is organized as follows: Section II gives the formulation of this analysis including assumptions, TMM description/build-up and the analysis cases considered. Section III presents a description and interpretation of the resulting analysis data. Section IV contains recommendations for further study and concluding remarks.

II. Formulation

A. Orion Spacecraft

The CEV spacecraft will be used for travel to the International Space Station (ISS), return to the moon, and future voyages to Mars. The Crew Module (CM) of the Orion CEV spacecraft is shown here in Fig. 1 and has a shape inspired by the Apollo spacecraft used in past lunar missions.

With the outer skin of the CM is removed, the pressure vessel is revealed as depicted in Fig 2. For this analysis, the pressure vessel is assumed to be composite.

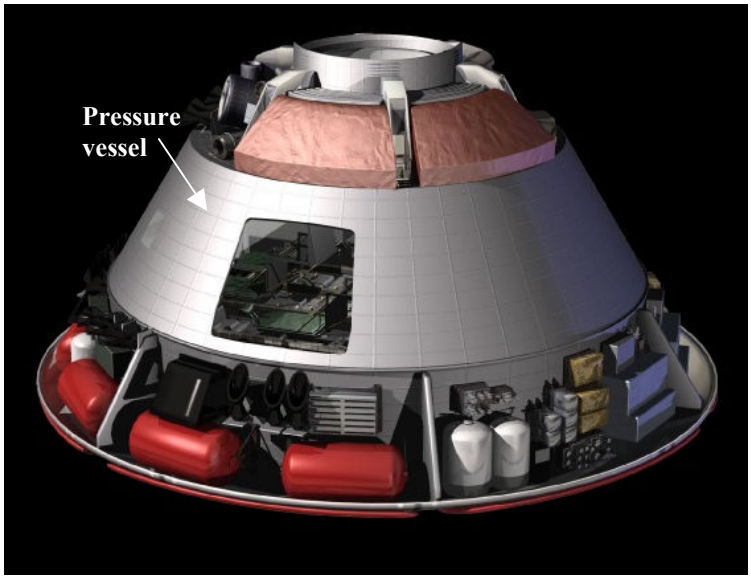

Figure 2. Crew module of the CEV with outer skin removed revealing the pressure vessel[2]

B. Composite Material

The schematic in Fig. 3 is representative of the CPV composite material configuration. The vessel cross section is composed of an inner face sheet (FS), outer FS, and honeycomb (HC) section.

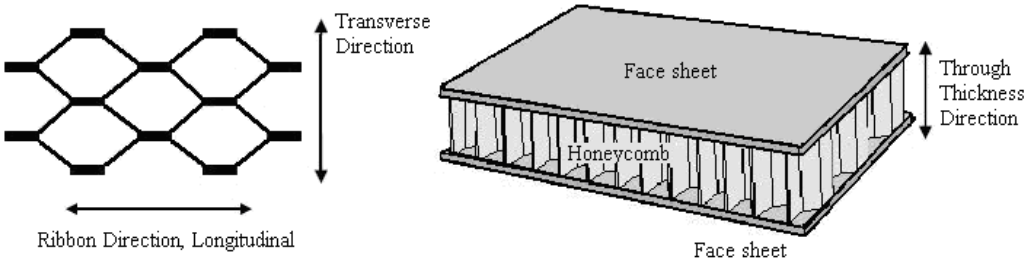

Figure 3. Honeycomb (HC) and inner and outer Face Sheet (FS) configuration[3]

The imported NASTRAN model assumed shell elements for the CPV structure. While this may be suitable for an aluminum crew module, the HC/FS could sustain larger thermal gradients through the thickness. Hence, the NASTRAN surfaces were extruded into solid elements and aggregate HC/FS conductance was assumed for the conductance in order to obtain the through-the-thickness HC/FS temperature gradient. Effective thermal conductivities were calculated for the different HC areas.

C. Assumptions

The optical properties used for radiative heat transfer calculations within the model are presented in Table 1. Multi-Layer Insulation (MLI) was used on the outer pressure vessel surface using an effective emissivity of ε^{*}=0.03. For this analysis, the lowest directional thermal conductivity was used for the inner and outer FS areas. The numbers of plies of fabric and tape that compose the different FS areas and determine its thickness were taken from the current NESC design specifications. The HC was assumed to be evacuated. To model the thermal conductivity through the composite shell, a JSC HC TMM was used for the different thickness sections of the HC area.

Table 1. CM Optical Property Assumptions

	Material Used	Solar Absorptivity, α	Infrared Emissivity, ε
TPS/Backshell Structure			
Outer BS	Reaction Cured Glass (RCG)	0.85 [Ref. 4]	0.85 [Ref. 4]
Outer HS	Reaction Cured Glass (RCG)	0.85 [Ref. 4]	0.85 [Ref. 4]
Inner FS	Titanium	N/A	0.2 [Ref. 5]
CPV			
Inner FS	Tape (M55J)	N/A	0.72 [Ref. 6]
Outer BS	Kapton Film, Aluminum Backing	N/A	0.71 [Ref. 7]

The inner CPV wall was set to 61.5°F (16.4°C) and energy was added to maintain each node at this temperature while not changing nodes that were already above the minimum temperature. Because the make-up energy was added at model nodal locations as opposed to over zoned regions, the impact of actual heater zoning is neglected. Hence, the full impact of heater power cannot be assessed until a zoning scheme is established and fully analyzed.

D. Model Description and Build-Up

The TMM incorporates a variety of different factors into the analysis. Once the conversion and augmentation of the finite element structure model was complete, the following subsystems were included in the TMM: Active Thermal Control System (ATCS), Avionics, Communications, Crew Systems, Electrical Power, Environmental Control, and Life Support System (ECLSS), Guidance, Navigation, and Control (GN&C), Landing and Recovery System (LRS), Mechanical System, Propulsion, and Structural. A graphic of the internal and external equipment associated with these CM subsystems along with the CPV are depicted in Fig. 4 and Fig. 5.

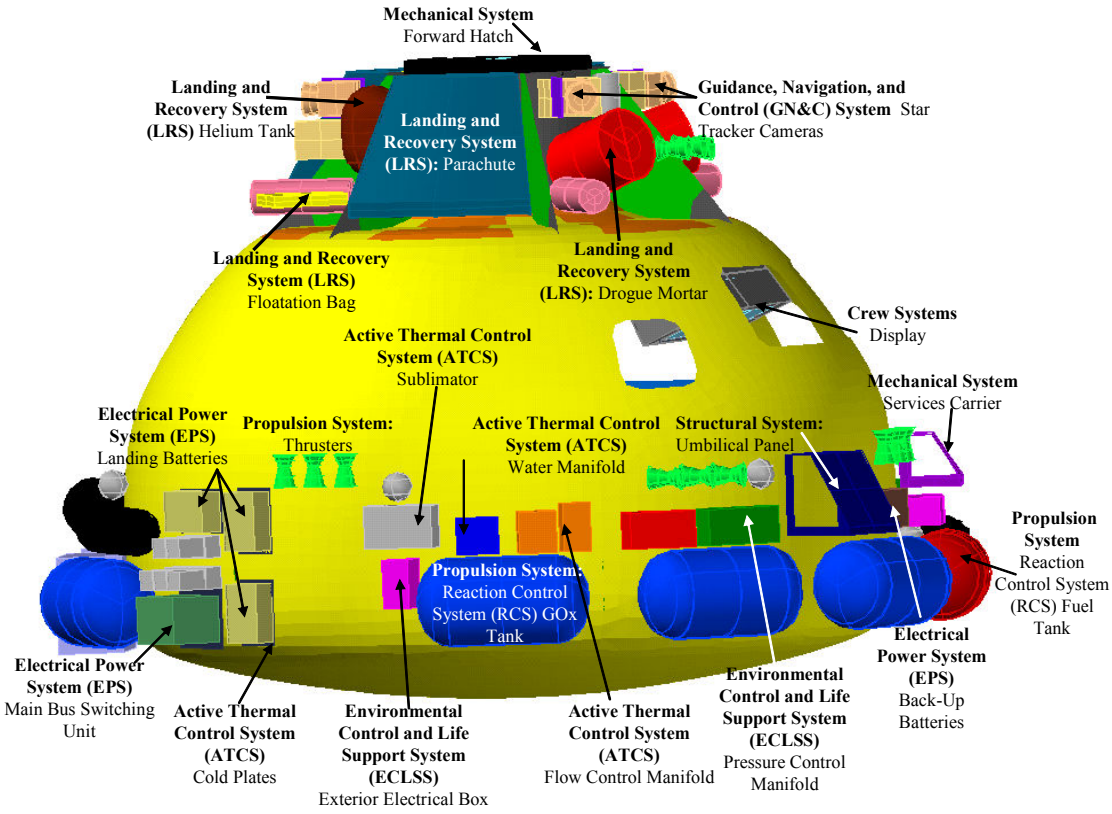

Figure 4. CPV with external subsystem components from TMM

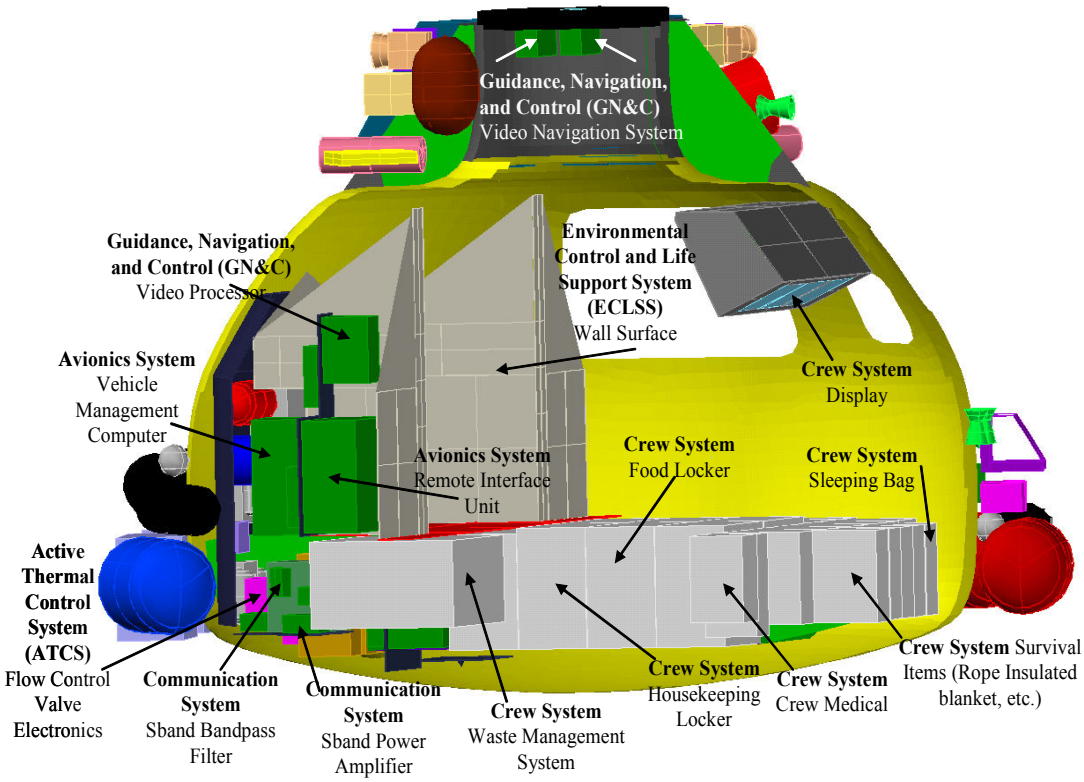

Figure 5. CPV with internal subsystem components from TMM

The Low Impact Docking System (LIDS) is used to dock the CM with the ISS. A graphical representation of the LIDS subsystem from the TMM is shown in Fig. 6.

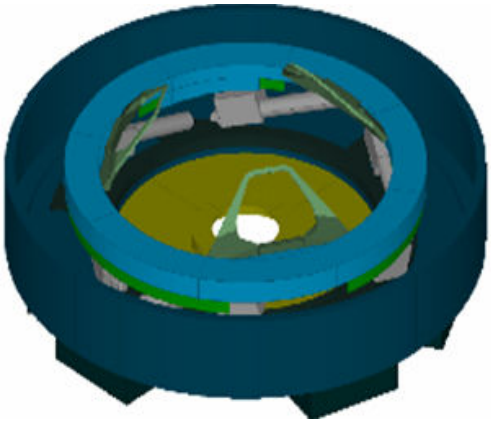

Figure 6. Low Impact Docking System (LIDS) TMM representation

Fig. 7 shows the Thermal Protection System (TPS) configuration of the CM included in the model. The TPS is composed of the Backshell (BS), and Heatshield (HS) and protects the module and crew from the re-entry heating.

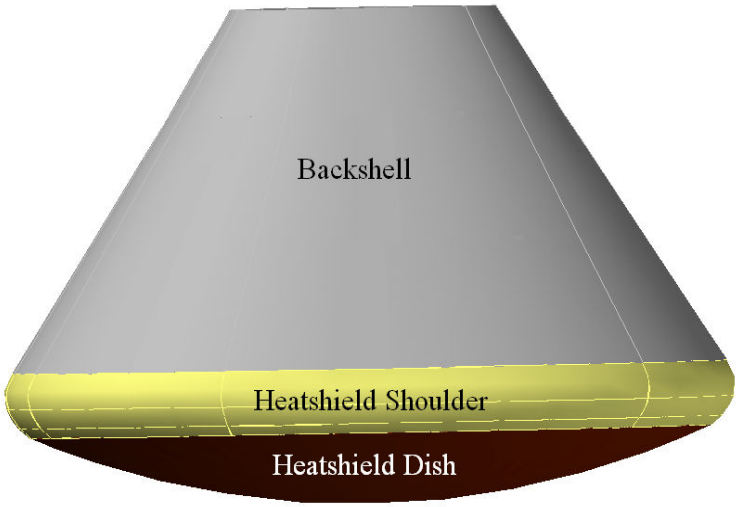

Figure 7. Thermal Protection System (TPS)

The TPS is a passive thermal control system with materials chosen based on thermal performance and weight efficiency. The backshell utilizes Alumina Enhanced Thermal Barrier (AETB)-8 tile. The heatshield is composed of Phenolic Impregnated Carbon Ablator (PICA). This layer is covering a layer of Room Temperature Vulcanized (RTV) material and Strain Isolation Pad (SIP). There is an underlying structural support composed of inner and outer Titanium FS with HC. Details of TPS stack-up configuration are shown in Table 2.

Table 2. Thermal Protection System (TPS)/Support Structure Stack-Up Thicknesses

Backshell (BS)	*Outer-most layer*:	0.63 in (1.6 cm) AETB-8 solid
		0.017 in (0.043 cm) Outer Ti FS
		0.75 in (1.9 cm) HC structure
	Inner-most layer:	0.017 in (0.043 cm) Inner Ti FS
HeatShield (HS) dish	*Outer-most layer*:	3.11 in (7.90 cm) PICA solid
		0.114 in (0.290 cm) RTV-SIP layer
		0.04 in (0.1 cm) Outer Ti FS
		2.4 in (6.1 cm) HC structure
	Inner-most layer:	0.04 in (0.1 cm) Inner Ti FS
HS shoulder	*Outer-most layer*:	2.5 in (6.4 cm) PICA layers (4)
		0.114 in (0.290 cm) RTV-SIP layer
	Inner most layer:	0.04 in (0.1 cm) Ti structure

Corresponding TPS thermophysical properties were taken from Refs. 8-12. As a simplification of this analysis, the SM was not explicitly included in this model. However, the effect of the SM blocking the heat shield from receiving direct view to deep space was simulated. Radiation conductors from the HS surface to an effective radiation node (ERN) at 50°F (10°C) were established in order to simulate the effect of the SM.

The CPV model contains 7755 planar elements and 7857 nodes. These CPV planar surfaces were extruded into solids and assigned an equivalent thermal conductance in order to capture through-the-thickness gradients within the honeycomb sandwich. The step by step procedure is shown in Fig 8.

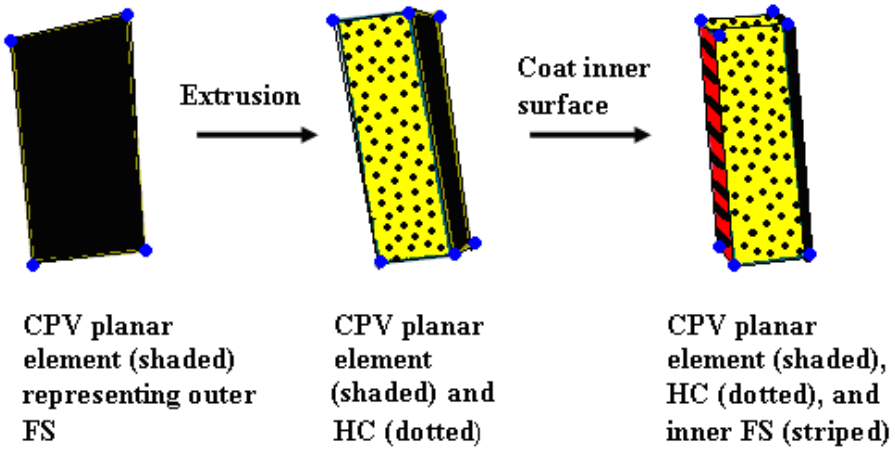

Figure 8. PV Thermal Desktop model building procedure

The shaded area represents the original shell CPV surface and was made to be the outer FS. The dotted area represents the extruded HC element. The striped surface represents the inner FS created by coating the inner surface of the HC. The HC/FS effective thermal conductivity was calculated based on the thicknesses of the HC/FS using an in-house JSC HC/FS TMM. Corresponding properties were applied to the CPV surfaces and solids. The sectioned areas of the HC/FS and corresponding thickness were chosen based on the current NESC design.

Longerons were assumed for the CPV structural support as shown in Fig. 9. These create a linear heat conduction path from the CPV to the surrounding inner TPS FS. The aggregate contact conductance for the longeron-FS areas used in the TMM were assumed to be 190 Btu/hr ºF (100 Watts/°C). This value includes contributions from all longerons along the total longeron surface area.

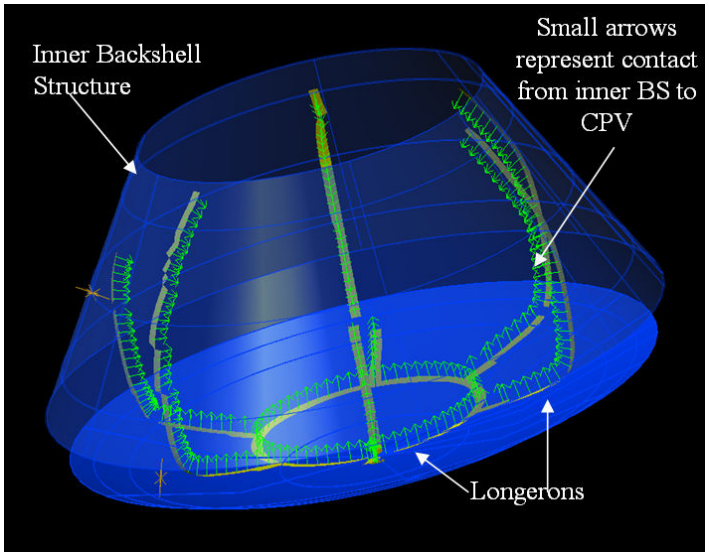

Figure 9. Assumed longeron structural support

Air nodes were created inside the CPV to account for the transfer of heat from the system components, through the air and to the CPV wall. There were 5 air nodes inside the CPV located as shown in Fig. 10.

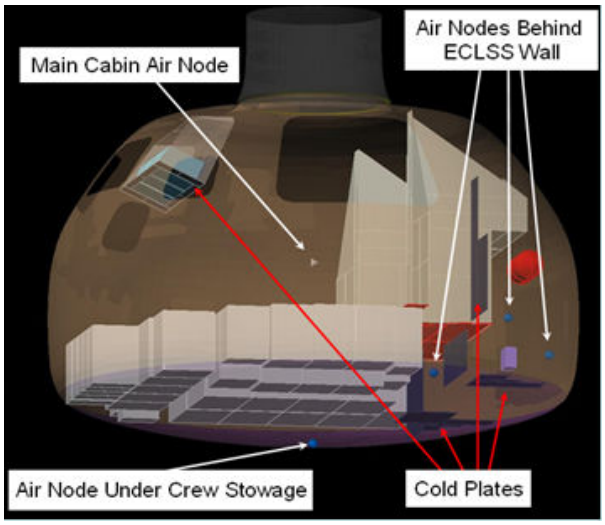

Figure 10. Location of Air Nodes and Cold Plates

The main cabin air node is maintained at 75°F (24°C). The cold plates are also shown in Fig. 10 and were set at 85°F (29°C). The estimated values for the unoccupied volumes surrounding each air node were taken from the current aluminum CEV baseline pressure vessel model. The values utilized are shown in Table 3.

Table 3. Estimated unoccupied volumes per current CEV baseline

Area	Volume (ft^3)	Volume (m^3)
Main	368.3	10.43
Port	18	0.55
Starboard	18	0.55
Center	42	1.2
Under crew stowage	51.5	1.46

The estimated total CPV volume is 718 ft^3 (20.3 m^3) based on the CEV baseline design. Figs. 11 and 12 show the air nodes coupling to the CPV structure and inner components.

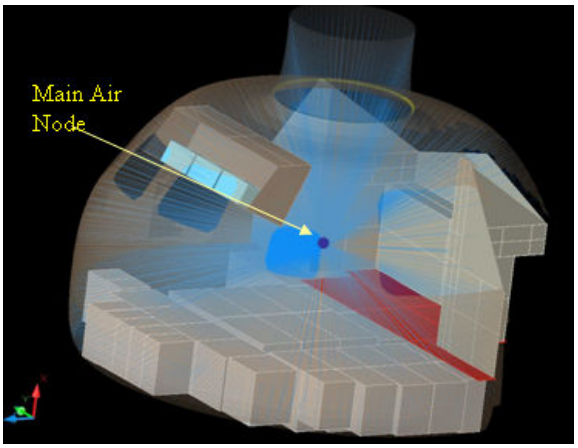

Figure 11. CPV main air node convection connections to surrounding PV wall and system surfaces

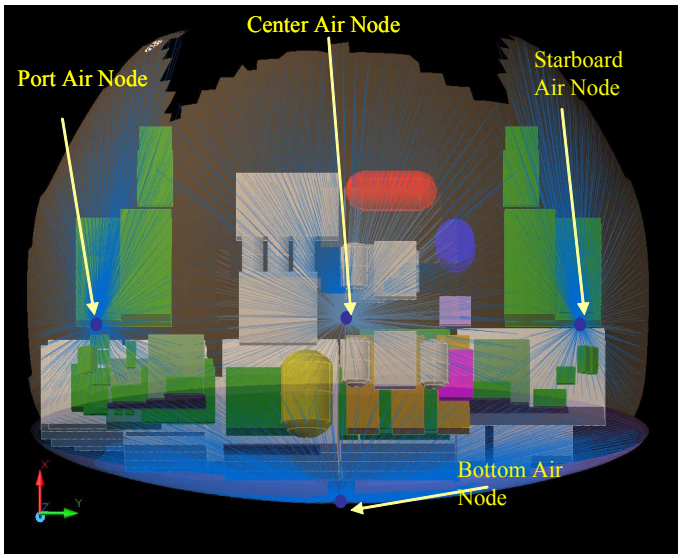

Figure 12: CPV port, starboard, center, and under crew stowage air nodes connection

The convective heat transfer coefficient representing air flow induced heat transfer in the bottom, center, port, and starboard sections of the CPV was assumed to be 0.25 Btu/hr/ft^2/°F (1.4 W/m^2/°C) and is typical of the value assumed for in-cabin convection on the Space Shuttle Orbiter. In the main cabin section of the CPV, the heat transfer coefficient was assumed to be 0.5 Btu/hr/ft^2/°F (3 W/m^2/°C) to account for the motion of the air. It should be noted that these convective heat transfer coefficients were not based on a computational fluid dynamics analysis. It is recommended that these coefficients be refined should additional analysis be performed. There is no direct coupling between air nodes. The total internal power dissipation is 7,582 Btu/hrs (2,222 W).

To calculate the make-up energy, specialized SINDA code was written and incorporated into the TMM. The model was configured to first run the steady state solution without any conditioning of the inner walls. This was the no make-up energy case and inner walls were allowed to trend to whatever temperature resulted from the overall heat balance (using SINDA diffusion nodes). Once the shell temperature distribution was determined for case without make-up energy, the program identified each node where the temperature was below the 61.5°F (16.4°C) limit. The program then altered these nodes to become heater nodes that were set and held at the limit. The remaining shell node locations remained unconstrained. The steady state solution was then re-run with these alterations to produce the results for the make-up energy case.

Four orbital configuration cases were chosen for this study based on an engineering judgement of which cases would likely cause the greatest high/low temperature extremes, and temperature gradients. Table 4 shows a breakdown of the analysis cases considered as well as its assumed characteristics.

Table 4. Orbital Configuration Analysis Cases

Case	Orientation	Natural Environments
Lunar transit, broad side to sun	The main axis of the vehicle is perpendicular to the sun vector. Half of the vehicle receives full, constant sun, the other half views deep space.	Hot solar flux. No albedo or Outgoing Longwave Radiation (OLR).
Lunar transit, aft to sun	The SM main engine faces the sun. Thus the entire CM is continuously shaded and sees deep space.	Cold solar flux. No albedo or OLR.
Low Lunar Orbit (LLO), nose to sun, Beta (β)=90°, 90 km altitude above lunar surface	The hatch/docking mechanism on the CM faces the sun full on.	Hot solar flux, albedo, and OLR.
LLO, aft to sun, β=90°, 90 km altitude above lunar surface	The SM main engine faces the sun. Thus the entire CM is continuously shaded and sees deep space. There is minimal albedo and OLR heating.	Hot solar flux, albedo, and OLR.

For the transit cases it is assumed that the spacecraft is sufficiently far from the Earth and moon such that there is no thermal influence from these bodies. Hence albedo and OLR are assumed 0.0 for these cases. For cases where the spacecraft was expected to experience colder conditions, the minimum solar constant value of 417.2 Btu/Hr/ft^2 (1315 W/m^2) was chosen as a conservative assumption. For cases where the spacecraft was expected to experience hot conditions, the maximum solar constant of 451.2 Btu/Hr/ft^2 (1422 W/m^2) was selected.

III. Results

Steady state temperature results for the four on-orbit analysis cases were produced in NASTRAN-compatible TEMP card format for direct input into the stress model. Temperature gradient maps were generated for each analysis case and are shown in Figs. 13-16. Fig. 13 shows the temperature distribution of the outer wall of the pressure vessel at steady state for broad side to sun, with a minimum inner wall temperature of 61.5°F (16.4°C). The effect of solar heating from the side that faces the sun throughout the orbit is displayed as a hotspot on the left view of Fig. 13. This hot spot is at approximately 148°F (64°C). The attachment points of the longerons to the CPV are demonstrated by the two cooler bands shown on the left view of Fig. 13.

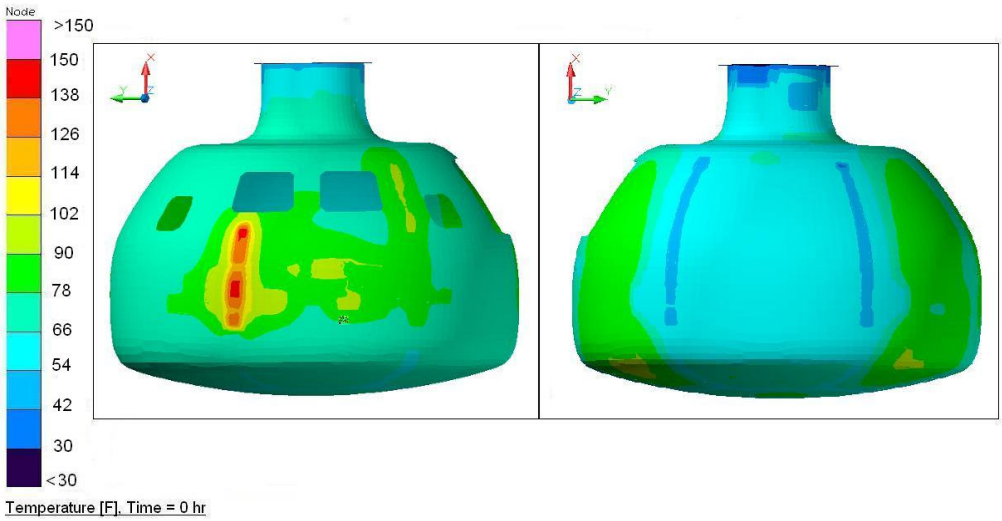

Figure 13. Steady State Temperature Results, Lunar Transit, Broadside to Sun, Minimum Inner Wall Temperature ≥ 61.5°F (16.4° C)

Fig.14 shows the steady state temperature results of a lunar transit case with the aft of the CPV pointed towards the sun throughout the orbit. The SM is located on the aft side of the CPV and prevents direct solar heating of the

CPV. The opposite side faces deep space through out the orbit. Therefore, we would expect to see some colder temperatures in these cases. There is a cold spot on the left view were the temperature reaches 5°F (-15°C). Here we see the impact of the through the thickness gradient that we initially expected. The inner FS temperature wall is maintained at a minimum of 61.5°F (16.4°C). The outer FS temperatures indicate a temperature of 5°F (-15°C) in some regions. The CPV in this area sustains a through the thickness gradient of ΔT=56.5°F (ΔT=31.4°C). This supports our initial assumption of a significant through the thickness gradient requiring extrusion of planar elements to account for this.

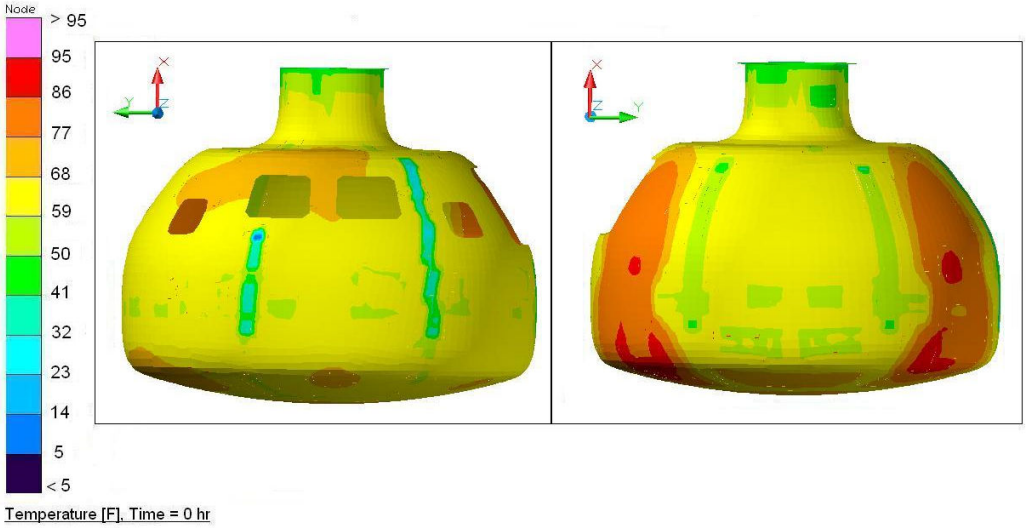

Figure 14. Steady State Temperature Results, Lunar Transit, Aft to Sun, Minimum Inner Wall Temperature ≥ 61.5°F (16.4°C)

Fig. 15 show steady state temperature results for low lunar orbit nose, nose to sun, β=90°, with a minimum inner wall temperature of 61.5°F (16.4°C). Note that as expected, the higher temperatures occur at the top of the CPV where exposure to solar heating is the greatest. The linear conduction through the longerons can be seen by the two yellow bands in the left and right view of Fig.15.

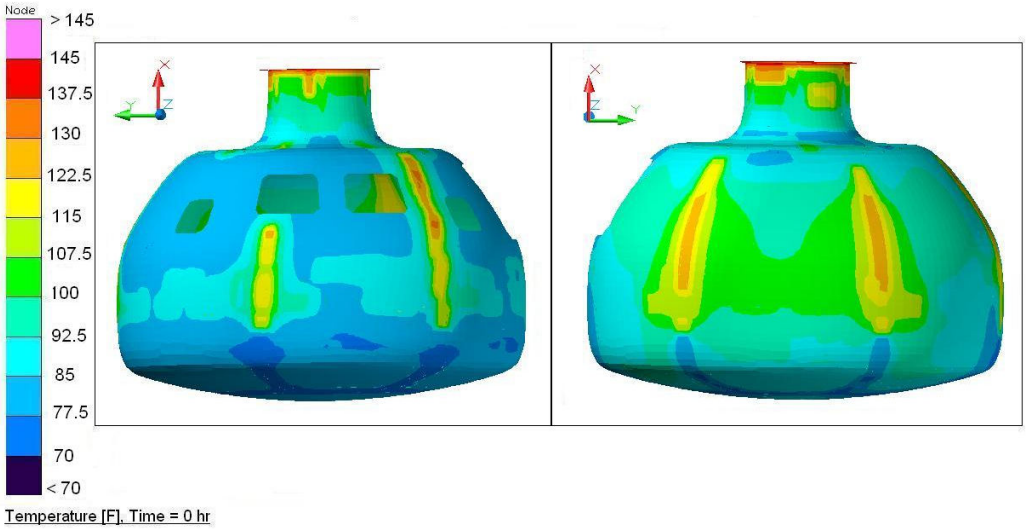

Figure 15. Steady State Temperature Results, Low Lunar Orbit, Nose to Sun, β=90°, Minimum Inner Wall Temperature ≥ 61.5°F (16.4°C)

Fig. 16 gives the temperature distribution results for the steady state case of low lunar orbit, aft to sun, β=90°, with a minimum inner wall temperature of 61.5°F (16.4°C). The through the thickness gradient is again seen here with the cold spot on the left view having a temperature of 10°F (-12°C). In this case the gradient is 51.5°F (28.4°C).

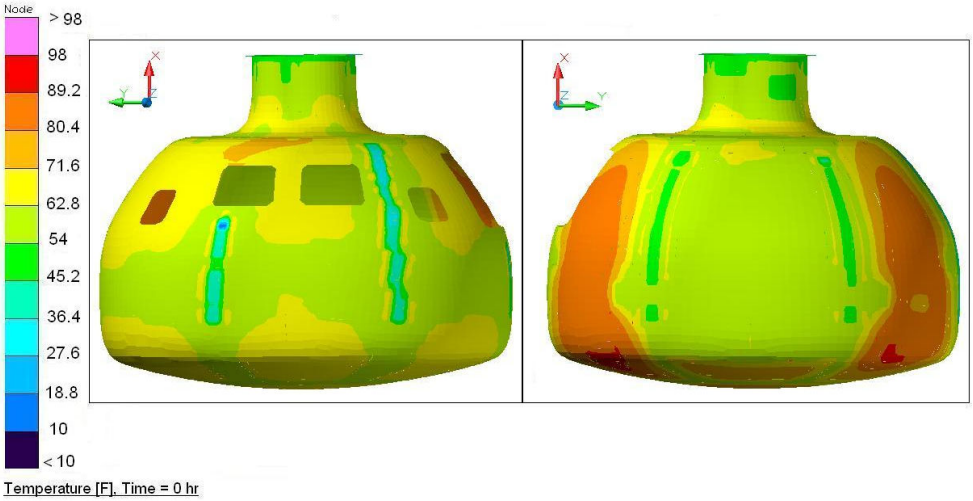

'igure 16. Steady State Temperature Results, Low Lunar Orbit, Aft to Sun, β=90°, Minimum Inner Wall `emperature ≥ 61.5°F (16.4° C)

The effect of adding make-up energy is shown in Figs. 17 and 18. Fig. 17 shows steady state temperature results for a lunar transit broadside to sun case. Without make-up energy, the gradients are more extreme showing temperatures at the cold spot of approximately -30°F (-34.4°C). With make-up energy, the temperature in these area increase to above 44°F (6.7°C). This is a significant increase and more realistic for the conditions that would be acceptable in an actual mission. Even though the inside is held to a 61.5°F (16.4°C) minimum temperature, the outside is below this limit due to the through the thickness gradient.

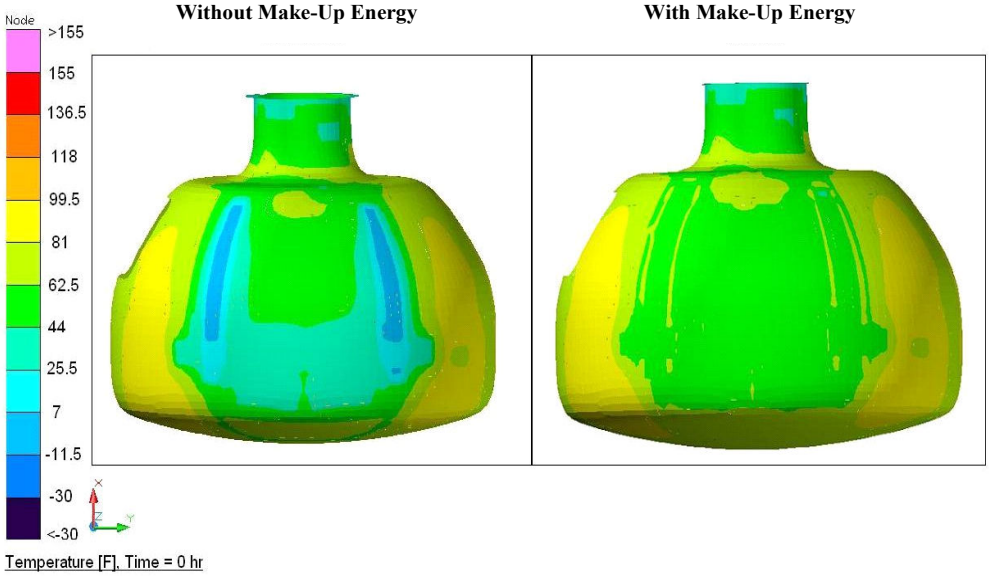

'igure 17. Effect of Make-Up Energy, Steady State Temperature Results, Lunar Transit, Broadside to Sun, =90°, Minimum Inner Wall Temperature ≥ 61.5°F (16.4°C) for Figure on the Right, No Minimum Inner Vall Temperature for Figure on the Left

Fig. 18 shows the effect of make-up energy for the steady state case of low lunar orbit, aft to sun. The cold spots on the left are removed with the application of make-up energy as seen in the view on the right.

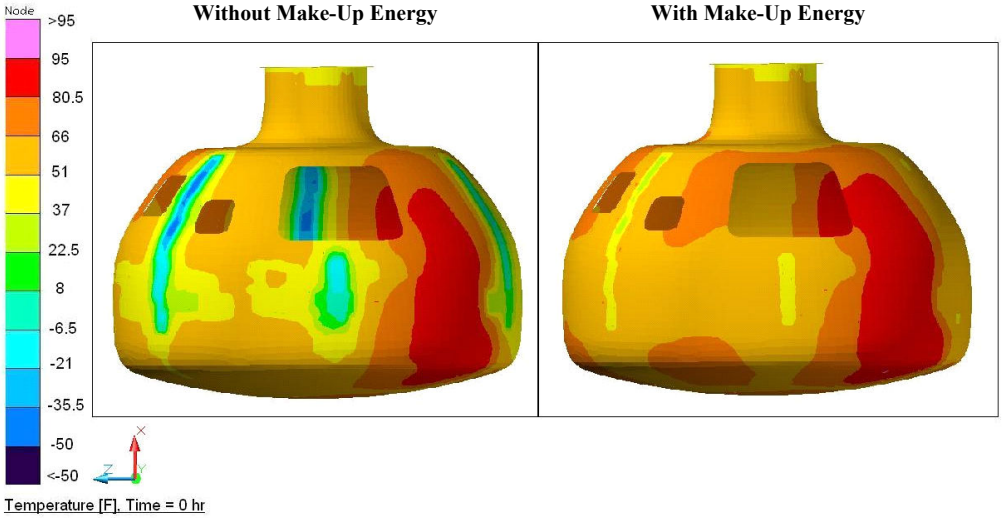

Figure 18. Effect of Make-Up Energy, Steady State Temperature Results, Low Lunar Orbit, Aft to Sun, Minimum Inner Wall Temperature ≥ 61.5°F (16.4°C) for Figure on the Right, No Minimum Inner Wall Temperature for Figure on the Left

IV. Recommendations and Conclusions

The temperature gradients seen in this analysis raise the question as to whether or not the associated thermomechanical stresses would create any performance issues. To address this question, further investigation to quantify the impact of thermomechanical stresses and its impact on overall design is recommended.

Taking in to account the original intent of this study, and the limited heater zoning data available, a solely qualitative overview of the make-up energy is given here to report the overall trends seen in the results. The results acquired suggest that the CPV requires significantly less make-up energy to hold the inner wall temperature above 61.5°F (16.4°C). On average around a 60% decrease in make-up energy requirement is indicated when using the CPV versus the aluminum pressure vessel. The greatest decrease was seen in the nose to sun case which indicated that no make-up energy is required to maintain the CPV above the 61.5°F (16.4°C) limit. This is a 100% decrease in the make-up energy requirements for the same case with an aluminum baseline pressure vessel. In the transit broadside to sun CPV case, a 70% decrease in make-up energy requirements was seen compared to the aluminum baseline case. Although not as prominent, a decrease also occurred in the transit aft to sun case and the low lunar orbit, aft to sun, β=90° case. These were on the order of a 30-40% decrease. Hence, this initial qualitative assessment uncovers the potential for a sizable energy savings by using the CPV instead of the aluminum pressure vessel. Although these results are promising, further refinement is recommended in order to conduct a more quantitative assessment of the observed gain. It is again emphasized that only local make-up energy was considered in the study. A heater zoning study to determine the configuration of the required heaters remains as future work. It is recommended that the baseline CEV heater design be incorporated into this model to enable an accurate comparison between using a pressure vessel of composite material versus aluminum. It is also suggested that some discussion within the community be initiated to assess whether the CEV baseline heater design would be used or whether a heater design specific to the CPV would be utilized.

Results of this thermal analysis suggest possible improvements to future analyses. A physical measurement of the composite sandwich aggregate thermal conductance is recommended so as to acquire a more accurate input for the model. It is recommended that lateral conductance within the CPV be considered by incorporating anisotropic conductivity values.

Acknowledgments

The authors wish to acknowledge Mike Kirsch, NESC Principal Engineer for providing the opportunity and guidance for this project. We also thank Jim Jeans, Genesis Engineering Solutions and Daniel Polis, NASA Goddard for providing us with CEV composite material properties and structural specification data, Stephen Miller,

CEV Passive Thermal Control System Manager for providing CEV baseline 605 modeling support and Alvaro Rodriguez for his composite material HC property calculation support. We recognize Mavis Brandt for her expert administrative support for coordinating the travel to meetings associated with this project. We would also like to express our appreciation for the support from Stephanie Matyas who provided extensive material property research assistance.

References

[1]JSC2007-E-20978, NASA image, May 2007.

[2]JSC2007-E-20979, NASA image, May 2007.

[3]Bednarcyk, B., Arnold, S., Collier, C., and Yarrington, P. "Preliminary Structural Sizing and Alternative Material Trade Study of CEV Crew Module," NASA/TM-2007-214947, 2007.

[4]Kourtides, D., Tran, H., and Chiu, S., "Composite Flexible Insulation for Thermal Protection of Space Vehicles," NASA /TM-1991-103836, 1991.

[5]Touloukian, Y. S., "Recommended values of the thermophysical properties of eight alloys, major constituents and their oxides, February 1, 1965 - January 31, 1966," NASA-CR-71699, 1966, p177.

[6]Amundsen, R., Dec, J., Gasbarre J., "Thermal Model Correlation for Mars Reconnaissance Orbiter," NASA Report 07ICES-64, 2007.

[7]Gilmore, D. (ed.), Spacecraft Thermal Control Handbook Volume 1: Fundamental Technologies, Aerospace Press, El Segundo, CA, 2002, p A-5.

[8]Design Specification for Natural Environments (DSNE) Document, NASA-CxP-70023, effective date August 2006.

[9]Natural Environments Definition for Design, NASA CxP 70044, effective date Aug. 2006.

[10]Space Shuttle Program Thermodynamic Design Data Book, Volume 3E, Book 1, Part 1, NASA SD73-SH-0226, Jan. 1981.

[11]Materials Property Manual, Vol. 3, Orbiter Specification MB0115-049, Boeing Company, Aug. 2005.

[12]Ed. T. Squire (ed.), "PICA", NASA TPSX Material Properties Database [online Database], Web Edition 4, Jan. 2006. <http://tpsx.arc.nasa.gov/>.